

UNCLASSIFIED

SECURITY CLASSIFICATION OF THIS PAGE

REPORT DOCUMENTATION PAGE				Form Approved OMB No. 0704-0183	
1a. REPORT SECURITY CLASSIFICATION Unclassified			1b. RESTRICTIVE MARKINGS		
2a. SECURITY CLASSIFICATION AUTHORITY			3. DISTRIBUTION/AVAILABILITY OF REPORT Approved for public release; distribution unlimited.		
2b. DECLASSIFICATION/DOWNGRADING SCHEDULE					
4. PERFORMING ORGANIZATION REPORT NUMBER(S) HDL-TR-2173			5. MONITORING ORGANIZATION REPORT NUMBER(S)		
6a. NAME OF PERFORMING ORGANIZATION Harry Diamond Laboratories		6b. OFFICE SYMBOL (If applicable) SLCHD-NW-EH		7a. NAME OF MONITORING ORGANIZATION	
6c. ADDRESS (City, State, and ZIP Code) 2800 Powder Mill Road Adelphi, MD 20783-1197			7b. ADDRESS (City, State, and ZIP Code)		
8a. NAME OF FUNDING/SPONSORING ORGANIZATION U.S. Army Laboratory Command		8b. OFFICE SYMBOL (If applicable) AMSLC		9. PROCUREMENT INSTRUMENT IDENTIFICATION NUMBER	
8c. ADDRESS (City, State, and ZIP Code) 2800 Powder Mill Road Adelphi, MD 20783-1145			10. SOURCE OF FUNDING NUMBERS		
			PROGRAM ELEMENT NO. 6.12.20A	PROJECT NO. XE78E5	WORK UNIT ACCESSION NO.
11. TITLE (Include Security Classification) A Comparison of the Diffracted Fields as Measured and Predicted for a Totally Reflecting Fence in a Scale Model Test for an EMP Simulator					
12. PERSONAL AUTHOR(S) James J. Loftus, Valerie Fronczak (Harry Diamond Laboratories), and Ira Kohlberg (Kohlberg Associates, Inc.)					
13a. TYPE OF REPORT Final		13b. TIME COVERED FROM 8/88 TO 1/89		14. DATE OF REPORT (Year, Month, Day) February 1990	
15. PAGE COUNT 28					
16. SUPPLEMENTARY NOTATION AMS code: 612120.H250011					
17. COSATI CODES			18. SUBJECT TERMS (Continue on reverse if necessary and identify by block number)		
FIELD	GROUP	SUB-GROUP	EMP scale modeling; EMP simulator; diffracted field prediction; Fresnel diffraction; diffracted field measurements.		
09	03				
20	14				
19. ABSTRACT (Continue on reverse if necessary and identify by block number)					
Experiments were conducted to observe and record the effectiveness of a fence acting as an electromagnetic barrier to the field emanating from a horizontally polarized electromagnetic pulse (EMP) simulator. The experimental results are compared to a theoretical model which predicts the observer height and range dependence of the electric field due to Fresnel diffraction. The comparison reveals good agreement, with typical uncertainties being on the order of 10 percent.					
20. DISTRIBUTION/AVAILABILITY OF ABSTRACT <input checked="" type="checkbox"/> UNCLASSIFIED/UNLIMITED <input type="checkbox"/> SAME AS RPT. <input type="checkbox"/> DTIC USERS			21. ABSTRACT SECURITY CLASSIFICATION Unclassified		
22a. NAME OF RESPONSIBLE INDIVIDUAL James J. Loftus			22b. TELEPHONE (Include Area Code) (703) 490-2420		22c. OFFICE SYMBOL SLCHD-NW-EH

## Contents

	Page
1. SUMMARY AND PURPOSE OF INVESTIGATION .....	5
2. BRIEF DESCRIPTION OF AESOP .....	6
3. ELECTROMAGNETIC SCALE MODEL EXPERIMENT .....	7
3.1 Background .....	7
3.2 Experimental Approach .....	8
3.3 Experimental Data .....	10
3.4 Supplemental Data .....	12
4. COMPARISONS BETWEEN THEORETICAL MODEL AND EXPERIMENTAL RESULTS .....	14
5. CONCLUSIONS .....	21
6. REFERENCES .....	22
APPENDIX.—EXPERIMENTAL ERROR .....	23
DISTRIBUTION .....	25

## Figures

1. Simulator, fence, and observer .....	5
2. AESOP pulser .....	7
3. Side and top view of AESOP and test area .....	7
4. Normalized AESOP pulse shape .....	7
5. Scale-model test area setup .....	9
6. Physical relationship between dipole and sensor .....	10
7. Physical relationship between dipole, metal sheet, and sensor .....	11
8. Sensor response to dipole, 10-ns data window .....	11
9. Sensor response to dipole, 2-ns data window .....	11
10. Sensor response to dipole field interrupted by a metal sheet .....	12
11. Leading-edge waveform of step-function generator .....	13
12. Sensor response to dipole step-function field .....	13
13. Sensor response to dipole step-function field with model fence in position .....	14
14. Sensor response to dipole step function field without model fence in position .....	14
15. Comparison between experimental and theoretical waveforms .....	16
16. Electric field in absence of fence for observer height = 7.5 m .....	17
17. Electric field in absence of fence for observer height = 15.0 m .....	17
18. Electric field in absence of fence for observer height = 22.5 m .....	17
19. Electric field in absence of fence for observer height = 30.0 m .....	17
20. Electric field in absence of fence for observer height = 37.5 m .....	17
21. Electric field in absence of fence for observer height = 45.0 m .....	17

## Figures (cont'd)

	Page
22. Comparison of $E_N$ and $\bar{E}_N$ in absence of fence .....	18
23. Electric field with fence for observer height = 7.5 m .....	19
24. Electric field with fence for observer height = 15.0 m .....	19
25. Electric field with fence for observer height = 22.5 m .....	19
26. Electric field with fence for observer height = 30.0 m. ....	19
27. Electric field with fence for observer height = 37.5 m .....	19
28. Electric field with fence for observer height = 45.0 m .....	19
29. Comparison between $E_F$ and $\bar{E}_F$ with fence .....	20
30. Comparison between electric-field ratios .....	20
31. Electric field in absence of fence, with 13.7-ns risetime and observer height = 22.5 m .....	20
32. Electric field with fence, with 13.7-ns risetime and observer height = 22.5 m .....	20

## Tables

1. Scale Model Facility instrumentation .....	8
2. Peak fields versus elevation, 3.5 m from dipole, with and without fence .....	13
3. Peak fields versus elevation, 7.0 m from dipole, with and without fence .....	13
4. Normalized experimental peak fields, with and without fence .....	15
5. Theoretical peak-field and ground time delay as a function of observer height in absence of fence .....	16
6. Theoretical peak field and ground delay as a function of observer height with fence .....	20
7. Comparison between experimental and theoretical electric-field ratios .....	20

Accession For

NTIS CLARI ☒

DTIC TAB ☐

Unannounced ☐

Justification

By \_\_\_\_\_

Distribution/

For \_\_\_\_\_

Dist \_\_\_\_\_

A-1

# 1. Summary and Purpose of Investigation

The Woodbridge Research Facility (WRF) of the U.S. Army's Harry Diamond Laboratories (HDL) conducts research and development of electromagnetic (EMP) simulators, and evaluates the effect of the simulated EMP on Army electronic and communications systems and subsystems [1].\* These simulated nuclear-generated pulses are characterized by risetimes on the order of nanoseconds, with decay times ranging from tenths to hundredths of nanoseconds. The energy is thus contained within a broad spectrum of frequencies.

The largest of the simulators at WRF is AESOP (Army EMP Simulator Operations), which can produce incident horizontal polarized peak fields of 50 kV/m at a ground range of 50 m from the simulator (see sect. 2). When the incident pulse is reflected by the ground, there will be constructive or destructive interference, the degree of which depends on range, observer height, ground conductivity, and ground dielectric constant. It is found that at large ranges, where the reflection coefficient is negative, there is an observer height regime where the time of arrival of the reflected field is less than the time to peak of the incident field. Under these conditions there is destructive interference and the peak of the incident field is not reached; this condition is defined as clipping. The degree of clipping depends on ground range, observer height, reflection coefficient, and waveform [2].

There is considerable interest in developing methods of reducing the peak electric field of AESOP (and thus for other simulators) that radiate beyond the boundary of the facility. One method under consideration is that of using an "EMP fence" made out of standard chain link. For example, if the chain link is bonded at every

aperture crosspoint, it has been shown that for the AESOP waveform the peak value of the electric field which penetrates through the fence is only 3 percent of the incident peak field [3]. Thus the fields which extend beyond the fence are due to diffraction over the fence. It is therefore of interest to determine these fields.

Such a fence could be located along the existing security fence line which is roughly parallel to, and approximately 175 m from, the AESOP antenna. The fence would be, by necessity, limited to a practical height of 20 to 25 m. Figure 1 shows a sketch of such an arrangement.

Although the fence appears to produce adequate field suppression on the outside by shielding, the field at distances greater than several hundred meters from the fence is determined by diffraction. The theory for predicting the time

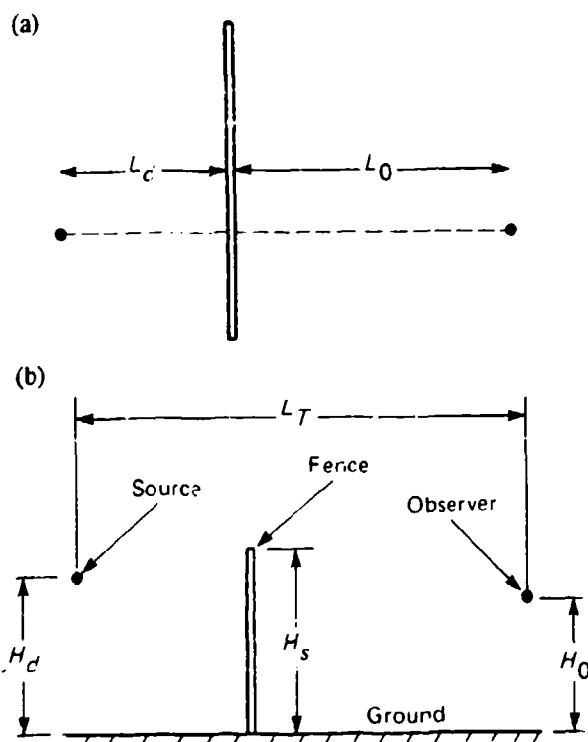


Figure 1. Simulator, fence, and observer: (a) top and (b) side.

\*References are listed at the end of the text.

behavior of the net field, including ground reflection, has been developed by one of us (I.K.) and is discussed elsewhere [3], as is the related computer program [4].

In this report we describe a scale-model experiment which was designed and conducted to test the concept of using a perfectly reflecting fence to suppress the AESOP far fields by diffraction. Because of the inherent difficulty of generating an accurate scaling of the shape of the AESOP waveform (see fig. 4) within the time constraints of setting up this experiment, we performed most of our testing with a scale model of AESOP but with a scaled time to peak,  $t_p$ , which is twice that of AESOP. Specifically, we have used a 1/50 scale model for the geometric dimensions of AESOP and the environment, and a scaled  $t_p$  of 0.400 ns. Strictly speaking the scaling law requires a value of  $t_p$  of 0.200 ns (which is the AESOP value, 10 ns, divided by 50). In the latter phases of the experiment we could however configure the pulser to achieve a real-world equivalent time to peak of 13.7 ns, which is close to the AESOP value of 10 ns. The details of the experimental setup and measurements are presented in section 3, while the corresponding comparison with theory is rendered in section 4. However, the major conclusions can be summarized as follows:

First, there was generally very good agreement between the theory and experiment, despite the differences in the shape of the experimental scaled waveform and the double-exponential scaled shape used in the theoretical model. This suggests that perhaps the peak fields are more sensitive to the time to peak rather than to the detailed structure of the early-time part of the waveform. This observation, however, must be tempered by the limited scope of the investigation.

For the conditions of the experiment, in which the fence is as high as the dipole source, we will achieve no more than a 50-percent reduction in the peak fields compared to the situation without the fence (the reasons for this are discussed in sect. 4). From a theoretical point of view, it would be possible to achieve a greater than 50-percent reduction in peak field strength by making the fence higher than the centerline of the simulator, but this would not appear to be practical. On the other hand, lowering AESOP would degrade its performance as a simulator. In summary, the scale-model experiment has established a quantitative assessment of the utility of a perfectly reflecting fence in reducing the far fields of AESOP-like simulators.

## 2. Brief Description of AESOP

The AESOPEMP simulator consists of a 300-m horizontally polarized dipole antenna and a 7-MV pulse generator. A 120- $\Omega$  biconic structure is used to launch the electromagnetic pulse. Figure 2 shows the AESOP pulser and biconic section. AESOP uses dual Marx generators, erected at opposite polarities to yield the net maximum of 7 MV of output.

Figure 3 shows the top and side view of the entire simulator and its relationship to the test region. For normal operations, the simulator is raised to a height of 20 m.

The incident horizontally polarized electric free field (also called the incident field) is adjustable to a maximum of 50 kV/m at a ground range of 50 m along the centerline at the AESOP elevation of 20 m. The centerline is that plane which is normal to the axis of the antenna, at the center of the pulser. Figure 4 shows the normalized AESOP pulse shape,  $f(t)$ . The pulse has a risetime of 10 ns, with the first zero crossing at 800 ns.

**Figure 2. AESOP pulser.**

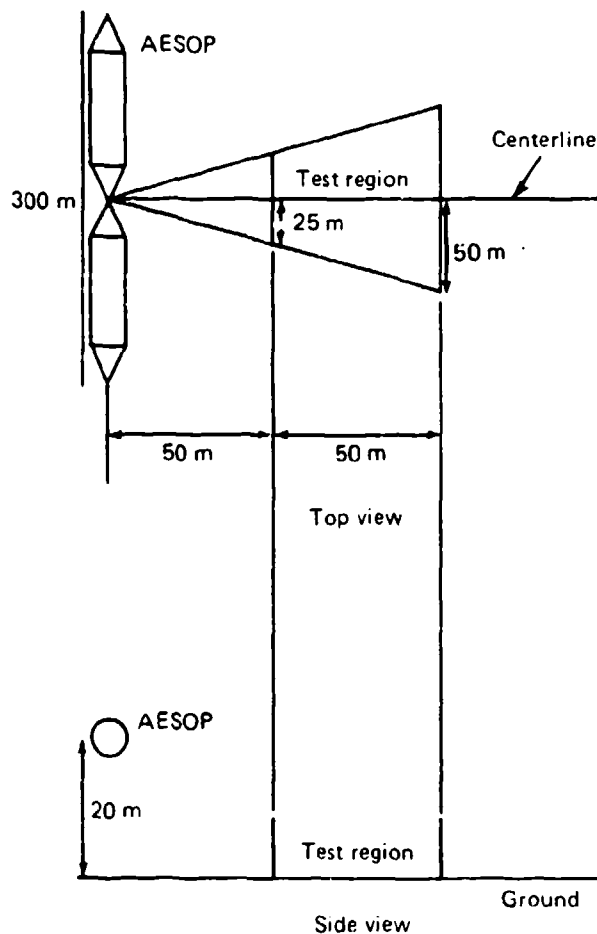
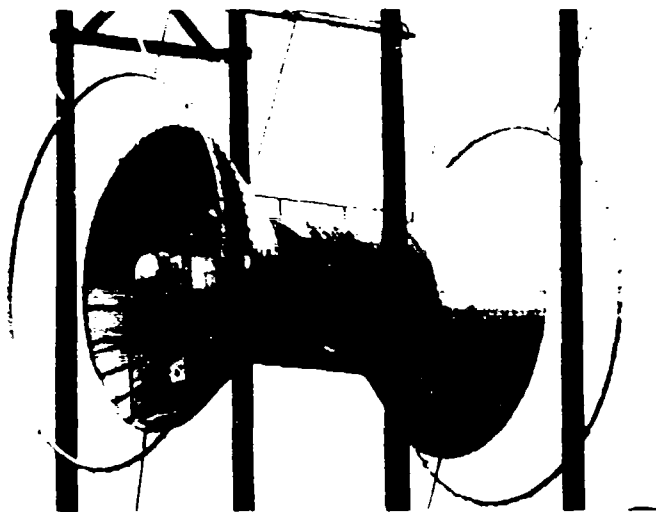


**Figure 3. Side and top view of AESOP and test area.**

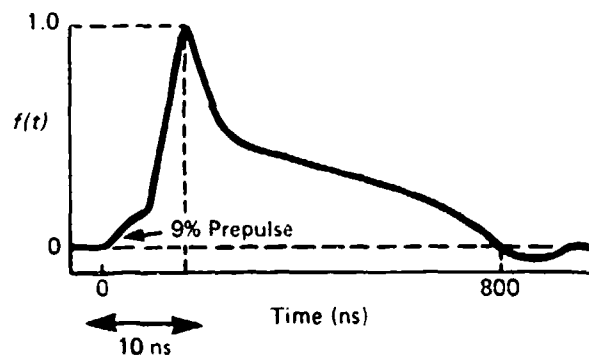


**Figure 4. Normalized AESOP pulse shape.**

### 3. Electromagnetic Scale Model Experiment

#### 3.1 Background

Electromagnetic scale modeling is possible because of the linearity of Maxwell's equations that describe the fields in any electromagnetic system. Sinclair [6] demonstrated that with the elimination of nonlinear media, it is theoretically possible to construct a model to simulate a full-scale system. This concept has been applied in many experimental studies, including coupling studies for Army electronic systems [7,8] at the HDL EMP Electromagnetic Scale Model Facility (SMF).

As stated, the AESOP simulator radiates a pulsed electric field with a risetime of 10 ns. The SMF can radiate a repetitive pulsed horizontal electric field with a risetime of 0.20 ns, which is approximately 1/50 that of AESOP. Models of military systems have been immersed in this field, and the recorded responses of their complex interconnecting external receptors have predicted with fair to good accuracy the corresponding full-scale system's responses when deployed at the AESOP simulator. Scale modeling of the proposed electromagnetic fence for AESOP was therefore a reasonable choice.

### 3.2 Experimental Approach

The instrumentation for these experiments is listed in table 1. A typical test setup at the model facility is shown in figure 5.

As a prelude to the detailed study to determine the peak field behavior as a function of observer height with and without a fence, we conducted a preliminary or "proof-of-principle" experiment to check out the salient features of the theory. It was desirable to ensure that our experimental design was consistent with the theory.

The theory [3] predicts that if a pulse-driven horizontal dipole radiator and a compatible electromagnetic sensor are arranged as shown in figure 6, the output of the sensor will decrease by approximately a factor of two if an interdicting sharp-edged metal body is placed between them, as presented in figure 7. A dipole antenna was attached to a repetitive pulse source, and an asymptotic monopole (D-dot) sensor was placed as shown in figure 6. The sensor was coupled to the recording instrumentation within the shielded enclosure through a high-quality coaxial cable. The pulsed field emanating from the dipole was recorded, as seen in figure 8. The data shown are from a 10-ns window which shows the computer-integrated sensor response converted to read as volts per meter versus time. The waveform was

**Table 1. Scale Model Facility Instrumentation**

Instrument	Comments
Sensors	D-dot, HDL, risetime < 0.15 ns B-dot, EG&G, risetime < 0.15 ns
rf cables	Andrews heliax cable
Pulse generators	Omni-Wave R-100, 1 kV into 50 $\Omega$ , pulse width = 0.15 ns  HDL Step 1, 1 kV into 50 $\Omega$ , risetime = 0.10 ns, length variable
Signal processor*	Tektronix WP-1221, including Digital processing oscilloscope, model 7704A Time-domain sampler, model 7612 Sampling head, model S-6 Trigger recognizer, model S-53  PDP-11 computer Display terminal Floppy disk unit Hard copy unit

\*Signal processor system bandwidth = 0.045 ns (10 to 90 percent)

intentionally recorded with a baseline, or zero sensor output, for the first nanosecond, at which time the leading edge of the wavefront is seen.

The radiated pulse from the dipole rises very quickly to about 38 V/m and has almost decreased to zero at  $T = 3$  ns, at which time the field may be observed to reverse polarity. This is the arrival of the ground reflection, that field which radiated from the dipole to the testbed sand to the sensor. The field was partially reflected and reversed in polarity by the conductive sand, as seen in the data. The calculated arrival time of this reflection is approximately 1.94 ns after the initial wavefront, or 2.94 ns in the data record. A calculation of the arrival time of the dipole "end effect," when the current on the dipole will reverse itself at the open ends, yielded an elapsed time value of 6 ns. In figure 8, the waveform reversal may be seen to occur about 6 ns from the baseline departure or when  $T = 7$  ns in the data window.

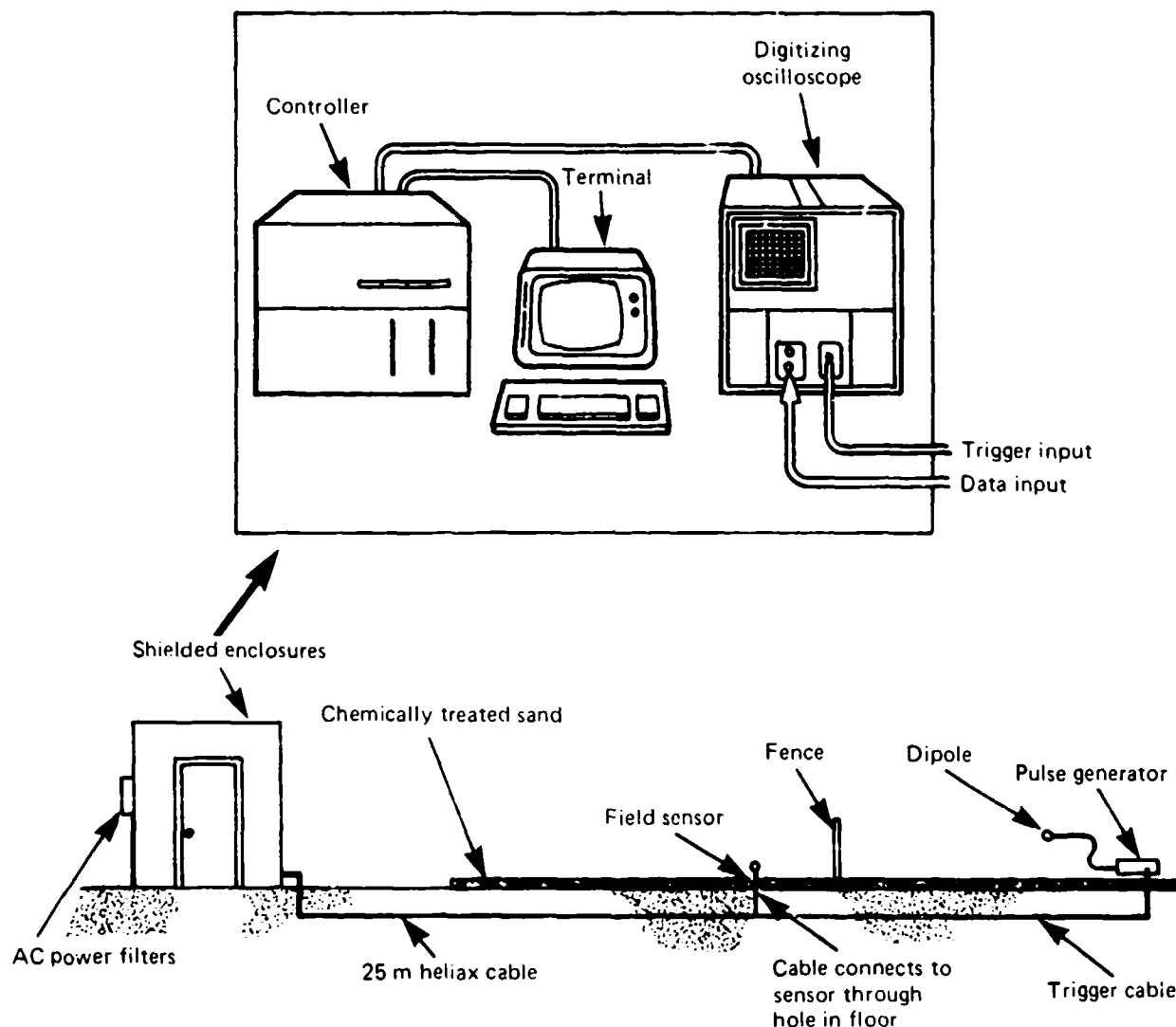


**Figure 5. Scale-model test area setup.**

The ground reflection and dipole "end-effect" arrival times have significance only in that the data demonstrate our ability to recognize where in time they should occur and may be observed. Figure 9 is a repeat of the measurement, recorded in a 2-ns data window for better definition. The peak of the field is clearly defined, and the effect of placing the metal sheet between the dipole and the sensor might now be observed.

The sensor output was again recorded after a sheet of metal was placed halfway between the dipole and the sensor, as seen in figure 7. The sensor height had been adjusted to that of the sheet

metal (0.84 m). The resulting data are presented in figure 10. The peak value of this waveform is approximately half that of the data recorded without the metal sheet in place (21/38 V/m). This ratio is consistent with the theory. The change in slant range between the dipole and the sensor for these recordings was insignificant, and since the ground reflection and end effects of the dipole may be ruled out, the metal sheet has caused the field to halve. As previously stated, this comparison of field measurements with and without a metal barrier was continued, using a scaled size metal sheet to represent the proposed fence, and scaled

Top View

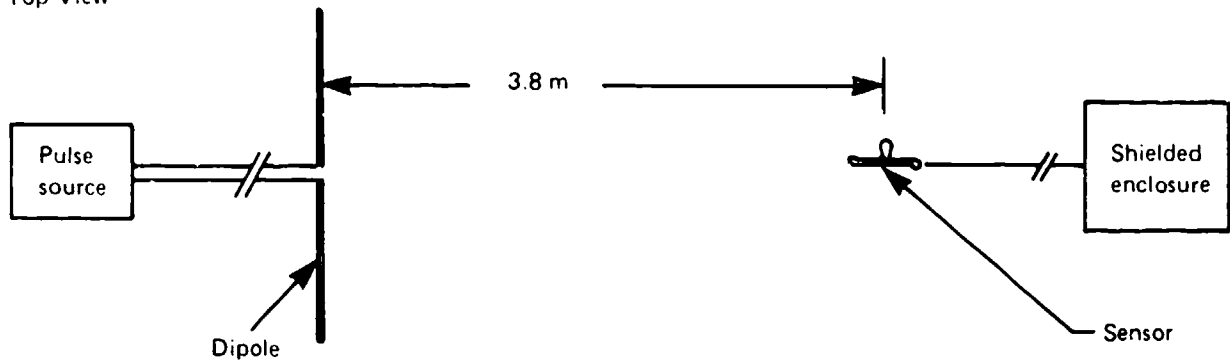


Figure 6. Physical relationship between dipole and sensor.

positions for the model elements which were 1/50 those of the AESOP test volume.

### 3.3 Experimental Data

The stated objective of the experiment was to observe and record the peak amplitude of a horizontally polarized pulsed field with and without a metal barrier, or fence, between the source dipole and a sensor. In this experiment, the spatial relationships of the elements of the model were hypothesized to be 1/50 of a real-world simulator such as AESOP. That is, where the AESOP simulator is normally positioned 20 m above the ground, the SMF dipole was 0.4 m above the testbed sand. Since the real-world distance between AESOP and the proposed fence would be approximately 175 m, the constructed model fence-to-dipole distance was 3.5 m. The dipole

was not a true model of AESOP, which is a somewhat complex structure composed of two opposite-polarity Marx generators, peaking capacitors, and a bicone/dipole radiator that is resistively terminated to the earth to minimize end reflections. AESOP radiates a pulsed field which approximates a double-exponential shape, but the concern of this experiment was solely with peak field values as affected by the fence. Field contributions from the model dipole ends, while inevitable, were of no concern.

The conductivity of the earth-simulating SMF testbed, which is composed of salt-treated sand, was adjusted to a value approximately 50 times that of the AESOP test area. The permittivity (and permeability) of the sand is approximately that of the earth, which is as required for modeling. A sheet of metal, with approximately 1/50 the dimensions of the proposed fence, was constructed

**Figure 7. Physical relationship between dipole, metal sheet, and sensor.**

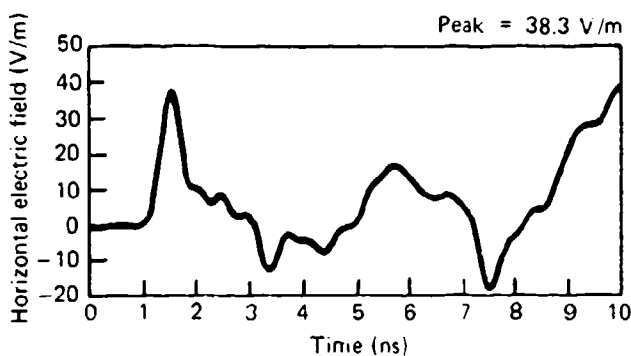
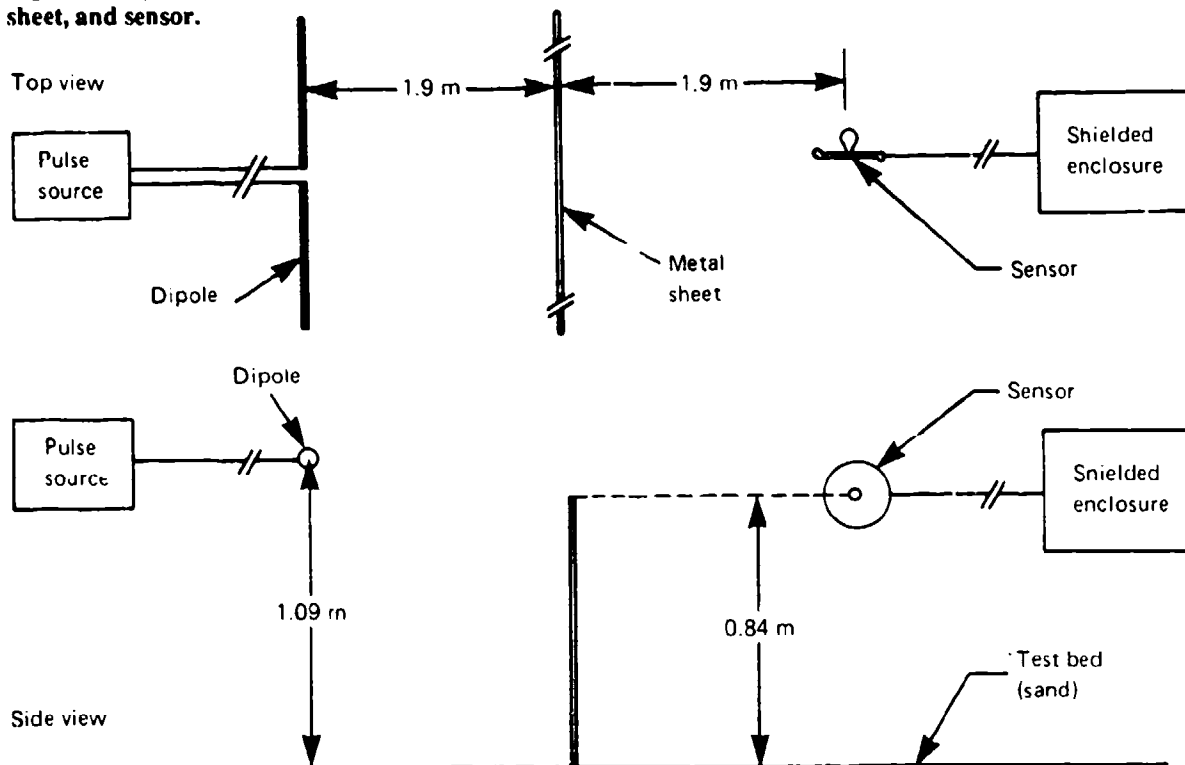


**Figure 8. Sensor response to dipole, 10-ns data window.**

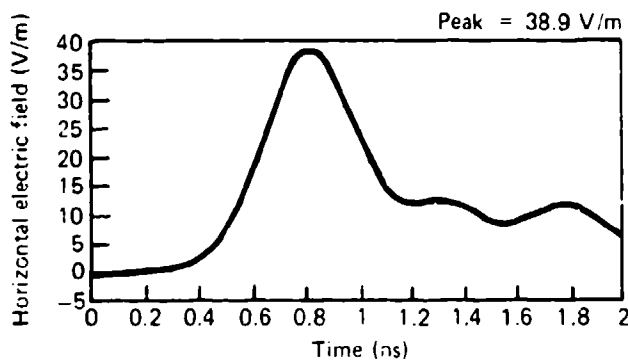


**Figure 9. Sensor response to dipole, 2-ns data window.**

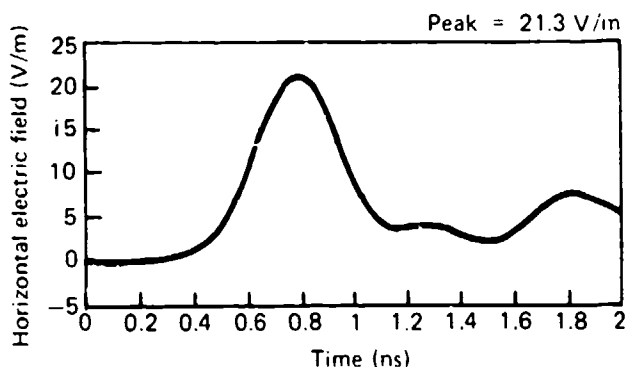


**Figure 10. Sensor response to dipole field interrupted by a metal sheet.**

for use with the previously fabricated dipole. The model fence was 7.3 m long and 0.46 m high, which corresponds to a real-world fence 365 m long and 23 m high.

The fields from the dipole were measured at ground-range distances of 3.5 and 7.0 m, with sensor-height variations from about 0.15 to 0.90 m, in 0.15-m increments. This corresponds to real-world ranges of 175 and 350 m, and height variations from 7.5 to 45 m. The 175-m position (referred to as position 1) corresponds to the property boundary behind AESOP, and the 350-m position (referred to as position 2) represents a location 175 m beyond that boundary. The measurements at position 1, when the sensor elevations were less than the fence height, were intended to determine the direct electromagnetic shielding achieved by the fence; in this zone, diffraction effects are minimal. The 350-m scaled position measurements were intended to evaluate the fields diffracted by the fence and are used for comparison to Kohlberg's theory [3].

The recorded peak fields for the resulting sensor responses at positions 1 and 2 may be seen in tables 2 and 3, respectively. These tables include the ratios of the "with fence" field values to the "no-fence" field values (see the appendix for a discussion of experimental error).

A comparison of these ratios and those produced by the FENCE program [4] may be found in

table 7, with a graphic presentation in figure 30 (see p 20). The time (to peak) of the field waveform in the FENCE program was 20 ns. This value was input to the program because although the scale-model radiated field measures to be approximately 0.20 ns, 10 to 90 percent, it is approximately 0.40 ns, zero to peak. In other words, we made the theoretical value used in the computer program equal to 50 times the experimental value. As may be seen from table 7, the ratios compare rather well, with the worst case (18 percent) being closest to the ground. This is reasonable, since the signal-to-noise ratio of the data decreases, as does the field, near the ground.

### 3.4 Supplemental Data

Our experience dictates that the more often one confirms theoretical predictions with physical measurements, the better. We decided to go further, and conduct a supplemental experiment to more closely model the original results as predicted by Kohlberg [3], where the time to peak of the theoretical pulse was 10 ns. This required a model pulse generator with a faster risetime.

A step-function generator was fabricated by HDL and substituted for the original pulse generator that drove the dipole. For several reasons, this pulse source could not be used at the inception of the experiments. The leading edge of this step function, as recorded through the cable that couples the generator to the dipole, may be seen in figure 11. The 10 to 90 percent measured risetime is  $\sim 0.150$  ns, while the zero-to-peak time is  $\sim 0.273$  ns. In scale, this corresponds to a zero-to-peak real-world time of 13.7 ns. While this is not exact, it is considerably faster than the original model pulse, which scaled to a 20-ns time to peak. With this pulse applied to the dipole radiator, we repeated several measurements to observe the effect. The dipole height was raised to that of the fence.

**Table 2. Peak fields versus elevation, 3.5 m from dipole, with and without fence**

Sensor height (in.)	Scaled height (m)	Peak fields (V/m)		WF/NF
		With fence (WF)	No fence (NF)	
~6	0.15	7.5	3.6*	~0.13
12	0.30	15.0	3.8*	~0.12
18	0.45	22.5	18.8	0.5
24	0.60	30.0	38.5	~1
30	0.75	37.5	37.9	~1
36	0.90	45.0	36.9	~1

\*Questionable data validity due to poor signal-to-noise ratio.

**Table 3. Peak fields versus elevation, 7.0 m from dipole, with and without fence**

Sensor height (in.)	Scaled height (m)	Peak fields (V/m)		WF/NF
		With fence (WF)	No fence (NF)	
~6	0.15	7.5	5.6	0.82
12	0.30	15.0	7.6	0.73
18	0.45	22.5	8.8	0.66
24	0.60	30.0	10.6	0.66
30	0.75	37.5	12.2	0.71
36	0.90	45.0	13.5	0.72

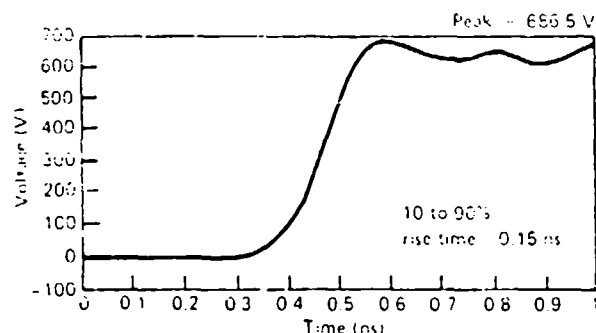


**Figure 11. Leading-edge waveform of step-function generator.**

The dipole field was measured as before, at a 7-m distance, with and without the fence present. Figure 12 shows the sensor response at a height of 36 in. (0.9 m) with the fence present. This figure includes two time windows, 2 and 10 ns. The calculated arrival time for the ground reflection is ~0.345 ns, and the 2-ns window data show clipping to occur at approximately this time. The end of the dipole field reversal may still be observed at ~6 ns in the 10-ns window data.

Figures 13 and 14 show the sensor response at an elevation of 0.45 m, with and without the fence. With the fence in place, the dipole, sensor, and top of the fence were all the same height above

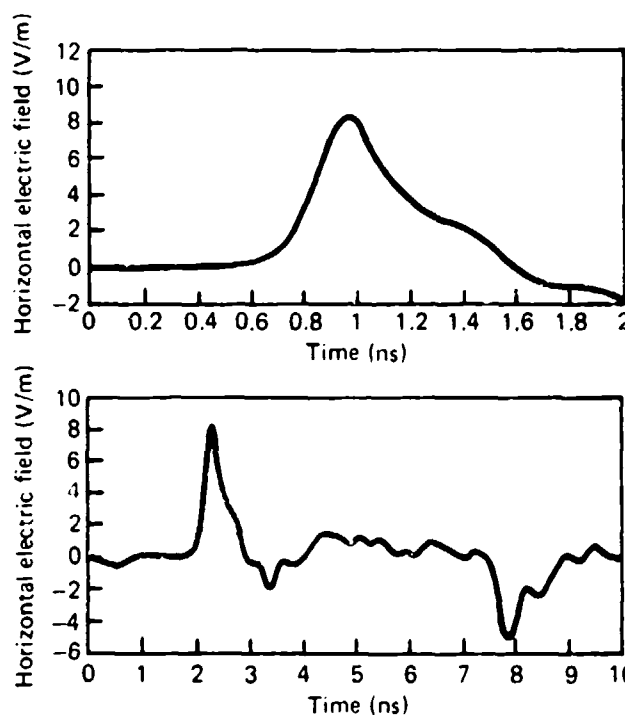


**Figure 12. Sensor response to dipole step-function field.**

ground.

The ratio of the peak of the fields for "with fence" to "no fence" is ~5/8.9 or 0.562. The ratio obtained with the computer program using a 13.7-

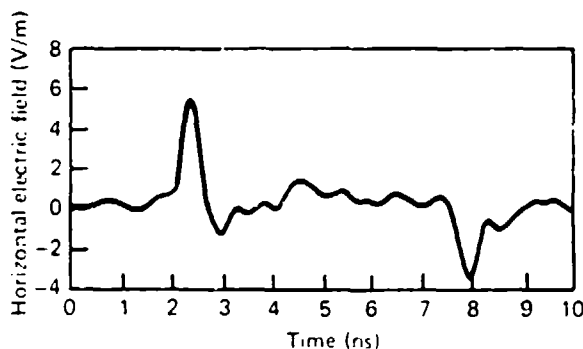
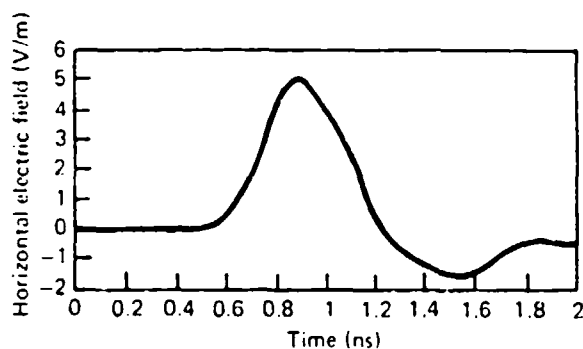


Figure 13. Sensor response to dipole step-function field with model fence in position.

ns risetime is 0.52. This can be compared with the earlier part of the experiment, in which the risetime was 400 ps (20 ns real world). At the same sensor height, the ratio obtained in the experiment was 0.66 (table 3), and the computer result was 0.61. The effectiveness of the fence is more evident with the faster risetime.

#### 4. Comparisons Between Theoretical Model and Experimental Results

This section compares the results of table 3 with theoretical predictions. Specifically, the following issues are addressed:

- (a) Dependence of peak field in absence of fence,  $E_N$ , as a function of sensor height.
- (b) Dependence of peak field with fence,  $E_F$ , as a function of sensor height.
- (c) Dependence of  $E_F/E_N$  as a function of sen-

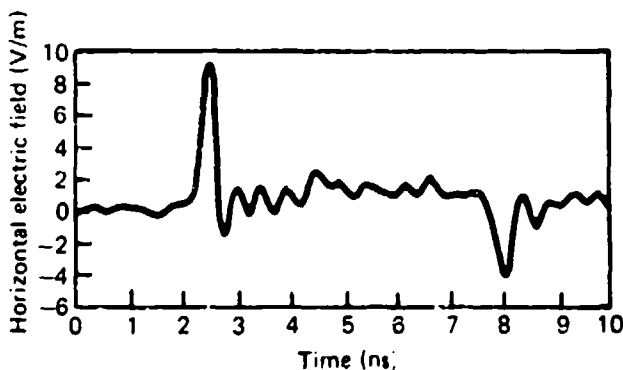
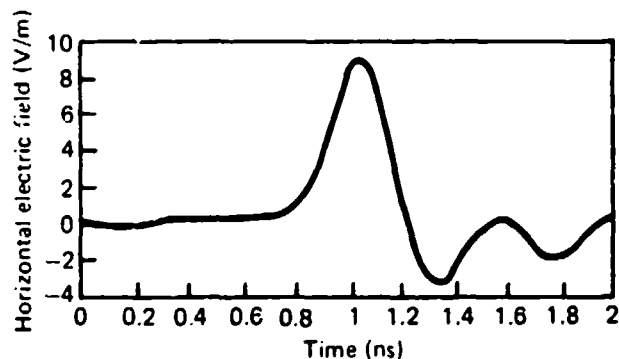


Figure 14. Sensor response to dipole step function field without model fence in position.

sor height.

(d) Extrapolation of this particular experiment, in which the sensor was 3.5 m from the fence, to cases where the sensor is much further from the fence.

To facilitate the comparison between theory and experiment, it is desirable to recast the experimental data of table 3 in an appropriately normalized form. The reason for this is that the absolute levels of the fields in the experiment are arbitrarily established by the input power to the dipole, while the absolute values of the fields calculated by the computer programs can also be arbitrarily set.

The normalization of the experimental data is calculated by dividing all the peak field-intensity measurements by the value of the no-fence case at the scaled height of 45 m. This value is 18.8 V/m (see table 3). Table 4 is a recasting of table 3 in normalized form (all dimensions are in real-world units).

**Table 4. Normalized experimental peak fields, with and without fence**

Height (m)	Experimental peak fields		$E_F/E_N$
	$E_F$	$E_N$	
7.5	0.30	0.36	0.82
15.0	0.40	0.55	0.73
22.5	0.47	0.71	0.66
30.0	0.56	0.85	0.66
37.5	0.65	0.91	0.71
45.0	0.72	1.00	0.72

The normalized values of fields  $E_F$ ,  $E_N$  are the values shown in table 3 divided by 18.8; that is,

$$E_F = \frac{(\text{WF value})}{18.8} \quad (1)$$

$$E_N = \frac{(\text{NF value})}{18.8}$$

As observed, the ratio

$$\frac{(\text{WF value})}{(\text{NF value})} = \frac{E_F}{E_N} \quad (2)$$

remains unchanged.

It is also more convenient to present the discussion in terms of the real-world dimensions rather than the experimental dimensions. For example, the model sensor height at 0.90 m will be regarded as the real-world dimension of 45.0 m. Likewise, the 0.40-ns zero-to-peak waveform used in the experiment should be interpreted as a 20-ns zero-to-peak waveform.

From a computational viewpoint it is not easy to express the actual experimental waveform in terms of a simple analytical expression which can be used in the FENCE [4] and REFLPROP [5] computer programs. These programs calculate the fields without and with the fence, respectively, and are constrained to use analytical expressions for the Fourier transforms of the input waveforms.

If we restrict our attention to the time domain before and including the peak of the experimental waveform, it is possible to provide an analytical approximation to the experimental waveform using

a mathematically generated double-exponential waveform. The normalized expression for the time behavior of the incident electric field is given by

$$E_o(t) = 1.05[\exp(-Bt) - \exp(-At)] \quad (3)$$

where  $t$  is in seconds and  $E_o$  will have a peak value of 1 V/m. The values  $B$  and  $A$  are the slow and fast time constants, respectively. The time for  $E_o(t)$  to reach its peak value of unity is given by

$$t_p = \frac{1}{A-B} \ln \frac{A}{B} \quad (4)$$

Using the values of

$$A = 86.0 \times 10^6 \text{ s}^{-1} \quad ,$$

$$B = 25.8 \times 10^6 \text{ s}^{-1} \quad ,$$

gives

$$t_p = 20 \text{ ns.}$$

Figure 15 compares the normalized double-exponential expression of equation (3) and the normalized model waveform. It is evident that the double-exponential waveform does not provide a very good approximation to the shape of the experimental waveform, other than in the agreement between the times to peak. Nevertheless, as we shall see in the comparison between theory and experiment,  $t_p$  appears to be perhaps the most important parameter in determining the peak value of the observed field.

Let us initially consider the comparisons between the behavior of  $E_N$  as a function of observer height and its theoretical counterpart, which we designate as  $\bar{E}_N$ . The height dependence of  $\bar{E}_N$  is determined from the computer program REFLPROP [8] using the normalized double-exponential waveform of equation (3). The calculated waveform is given by

$$\bar{E}_N(\Delta) = E_o(\Delta) + E_i(\Delta - T_L) \quad (5)$$

where  $E_o(\Delta)$  is given by equation (3) with  $t$  replaced by the retarded time,  $\Delta$ ;  $E_r$  is the ground-reflected contribution; and  $T_L$  is the time delay between the incident and ground reflected waves. The ground response is defined for  $\Delta \geq T_L$ . The retarded time,  $\Delta$ , is given by

$$\Delta = t - \frac{R_o}{c} \quad (6)$$

where

$$R_o = [L^2 + (H_d - H_o)^2]^{1/2}, \quad (7)$$

$L$  is the ground range between source and observer,  $H_d$  is the dipole (AESOP) height,  $H_o$  is the height of the observer, and  $c$  is the velocity of light.  $R_o$  is the line-of-sight distance between the source and observer. If the ground range is considerably greater than the sum of the heights, then the time delay,  $T_L$ , is given by

$$T_L = \frac{2H_d H_o}{cL}. \quad (8)$$

For the conditions of the experiment, the ground reflection coefficient is approximately  $-1$ , and  $E_r(\Delta - T_L)$  is given by

$$E_r(\Delta - T_L) = -E_o(\Delta - T_L). \quad (9)$$

When equation (9) applies and the reflection time delay is less than the time to peak of the incident wave, the net peak field occurs at the onset of the reflected wave and is given by

$$\bar{E}_N = E_o(T_L). \quad (10)$$

Table 5 gives values of  $\bar{E}_N$  and  $T_L$  for the real-world conditions of the experiment, as determined from REFLPROP. Figures 16 to 21 show the waveforms corresponding to the conditions of table 5. In all cases there is clipping of the direct

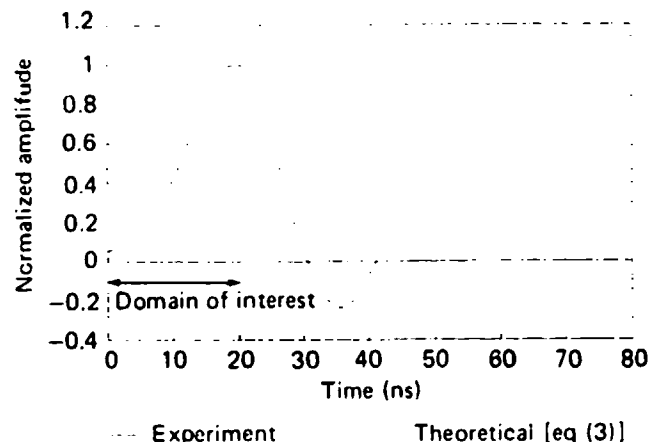


Figure 15. Comparison between experimental and theoretical waveforms.

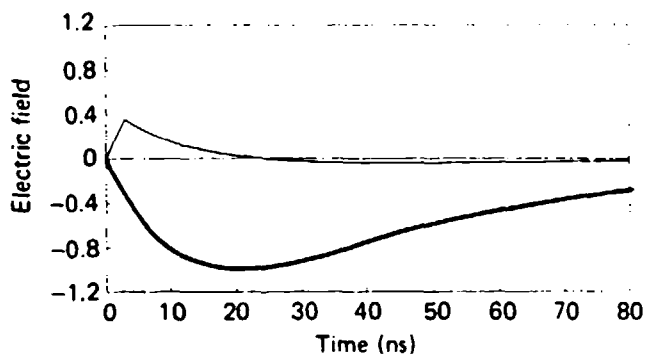
Table 5.  
Theoretical peak-field and ground time delay as a function of observer height in absence of fence

Height (m)	$\bar{E}_N$	$T_L$ (ns)
7.5	0.33	2.9
15.0	0.60	5.7
22.5	0.78	8.6
30.0	0.88	11.4
37.5	0.96	14.3
45.0	1.00	17.0

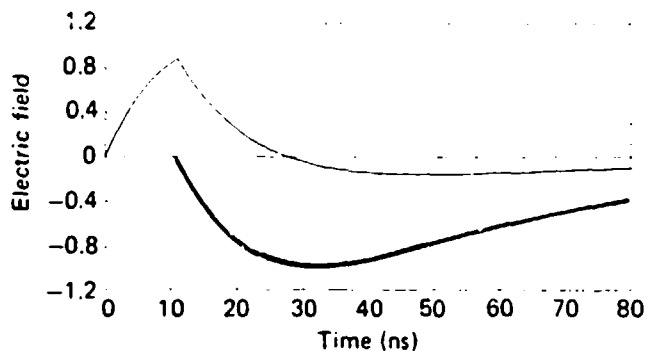
field since the time of reflection arrival is always less than  $t_p$ . As observed, the peak field,  $\bar{E}_N$ , occurs at the onset of ground reflection and is consistent with equation (8). This clipping effect is an important consideration in field reduction at large distances and at low observer heights, as can be seen from equation (10).

Figure 22 compares the normalized experimental and theoretical values of peak field. These curves are obtained from the values of  $E_N$  and  $\bar{E}_N$  given in tables 4 and 5, respectively. There appears to be good agreement between the curves.

We now turn our attention to the fence case. From a theoretical point of view, we once again begin with the normalized waveform. That is, we retain the same incident field levels as in the no-fence case; this is consistent with the way it was done in the experiment. The theoretical value of the field, designated by  $\bar{E}_r$ , is calculated from the FENCE computer program.



**Figure 16. Electric field in absence of fence for observer height = 7.5 m.**



**Figure 19. Electric field in absence of fence for observer height = 30.0 m.**

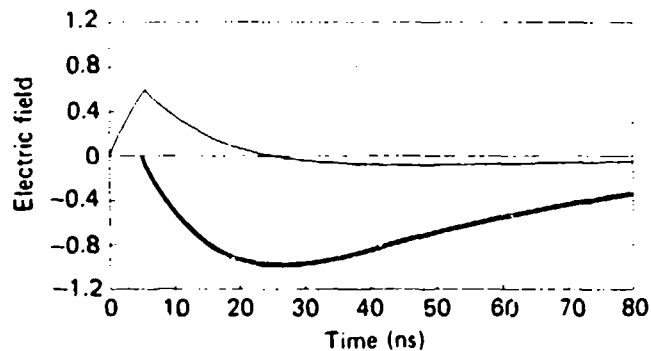


**Figure 17. Electric field in absence of fence for observer height = 15.0 m.**

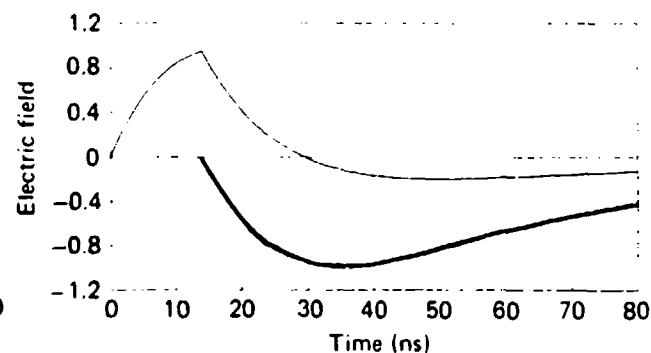


**Figure 20. Electric field in absence of fence for observer height = 37.5 m.**

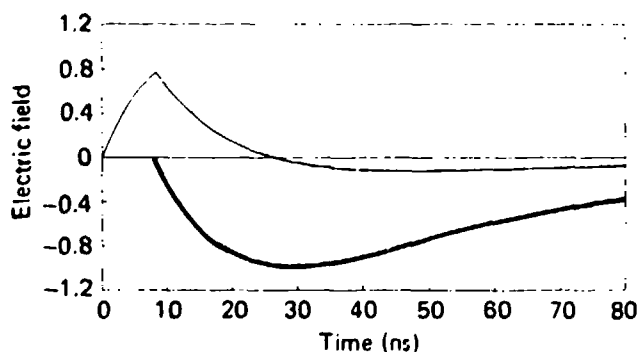


**Figure 18. Electric field in absence of fence for observer height = 22.5 m.**

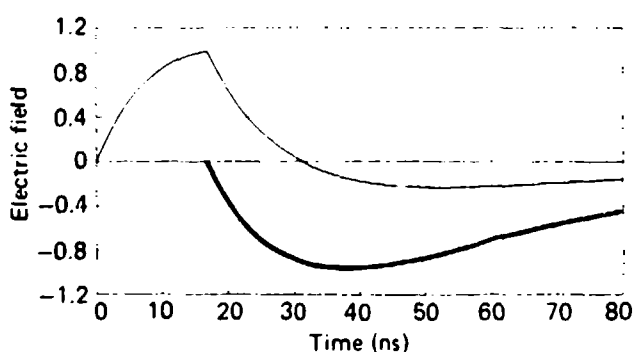


**Figure 21. Electric field in absence of fence for observer height = 45.0 m.**

The resulting waveform in this case is given by

$$\bar{E}_F(\bar{\Delta}) = I_d(\bar{\Delta}) + I_i(\bar{\Delta}) \quad (11)$$

where  $I_d(\bar{\Delta})$  and  $I_i(\bar{\Delta})$  are the contributions from the direct diffracted ray and the external diffracted reflected ray (image), respectively. The direct diffracted ray is from the source to the fence top to the observer. The external diffracted reflected ray is from source to fence top to ground to observer. The time behavior of the field at the selected point is calculated in terms of the ground delay time  $\bar{\Delta}$ , given by

$$\bar{\Delta} = \frac{t - L}{c} \quad (12)$$

where, as before,  $L$  is the ground range between source and observer.

The retarded time,  $\bar{\Delta}$ , is introduced for computational convenience. It should be noted that except for the special case in which both the source and the observer are at the same height, and both are higher than the fence, the onset of the field will begin at  $\bar{\Delta} > 0$ .

Figures 23 to 28 show the waveforms with the fence present, as computed from the FENCE program. As in the no-fence case of figures 16 to 21, the net peak fields occur at the onset of the image (ground reflected) contribution. There is also a time delay between the direct and image waves,  $T'_L$ , which is approximately given by

$$T'_L \cong \frac{2H_f H_o}{cL_o} \quad (13)$$

where  $H_f$  is the height of the fence and  $L_o$  is the distance between the fence and observer.

Table 6 shows the theoretical peak field ( $E_F$ ) corresponding to figures 23 to 28 and the corresponding ground time delay ( $T'_L$ ) at the measured heights when the fence is present.

Figure 29 compares  $E_F$  (table 4) and  $\bar{E}_F$  (table 6) in the presence of the fence. As ob-

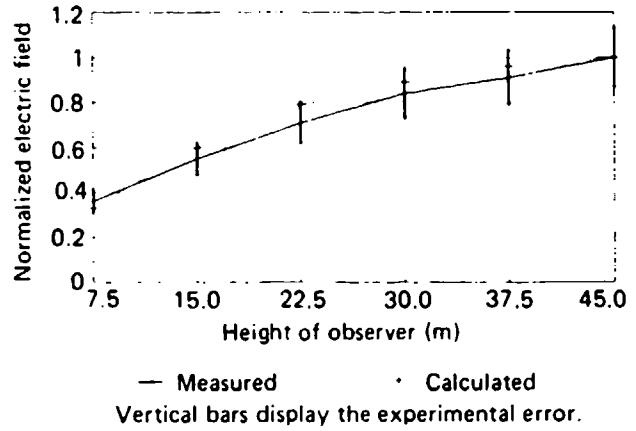


Figure 22. Comparison of  $E_N$  and  $\bar{E}_N$  in absence of fence.

served, there appears to be relatively good agreement between the curves. It would appear that the differences between the curves are within the experimental uncertainties (see app A).

Of particular importance in evaluating the utility of the fence is the ratio  $E_F/E_N$  as a function of observer height. Table 7 and figure 30 show this ratio along with the theoretical value  $\bar{E}_F/\bar{E}_N$ . Here again, the comparison falls within the uncertainties of the experiment. Although the results of figures 22, 29, and 30 support the theoretical model, the numerical values of  $\bar{E}_F/\bar{E}_N$  indicate that the fence does not greatly reduce the field intensity for the conditions of the experiment. The reason for this is that the no-fence case permits relatively more clipping of the incident field than does the fence case.

When the relative effect of clipping is reduced, which occurs when  $t_p$  is reduced, the fence has a relatively more beneficial effect. Using the 13.7-ns waveform previously discussed with  $H_f = H_o = 22.5$ , it is found that  $E_F/E_N = 0.56$ , while the theoretical value is 0.52. Figures 31 and 32 show the no-fence and fence cases, respectively, corresponding to the 13.7-ns waveform.

Theoretical estimates of the benefits of a fence are presented elsewhere [3], where it is noted that over a large range of observer distance and height, the ratios of  $\bar{E}_F/\bar{E}_N$  fall in the range of 0.45 to 0.55

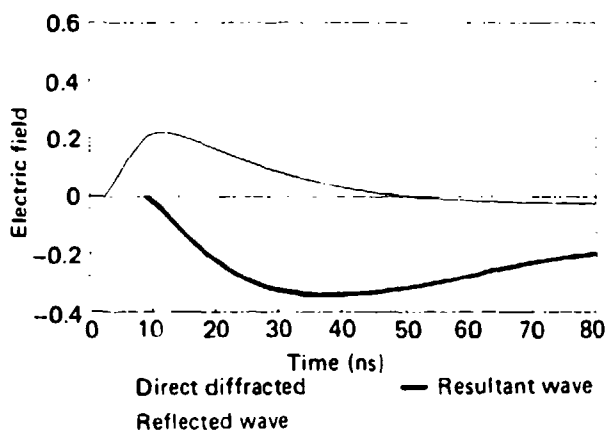


**Figure 23. Electric field with fence for observer height = 7.5 m.**

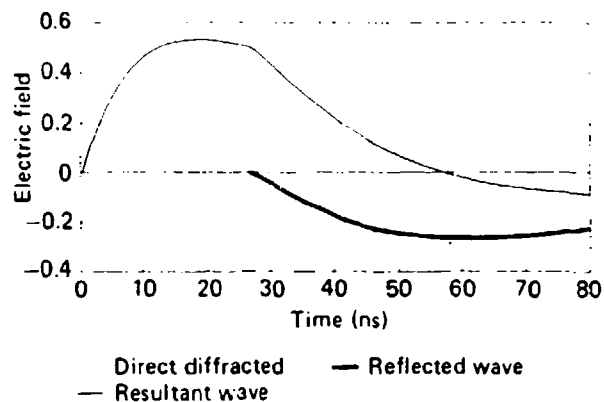


**Figure 26. Electric field with fence for observer height = 30.0 m.**

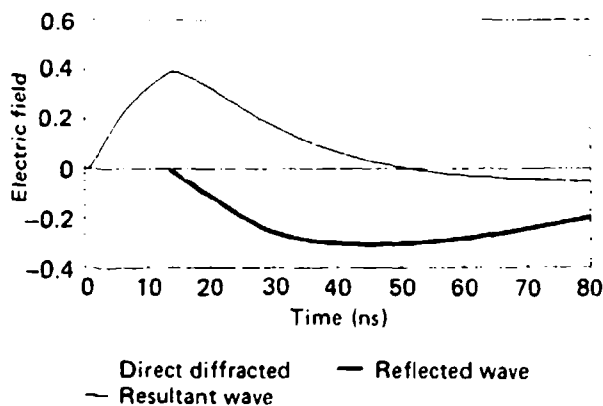


**Figure 24. Electric field with fence for observer height = 15.0 m.**

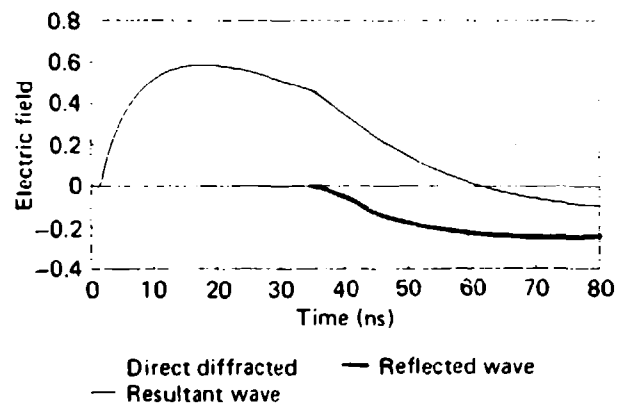


**Figure 27. Electric field with fence for observer height = 37.5 m.**

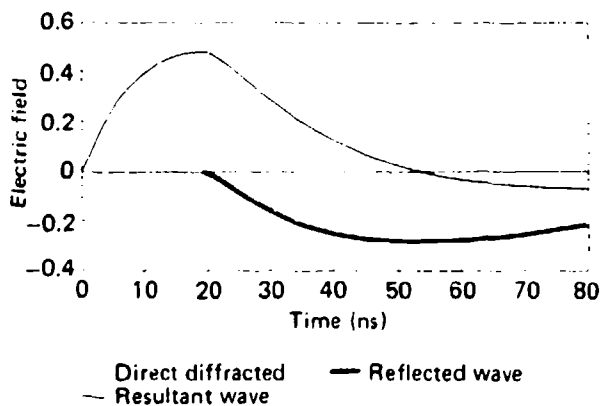


**Figure 25. Electric field with fence for observer height = 22.5 m.**

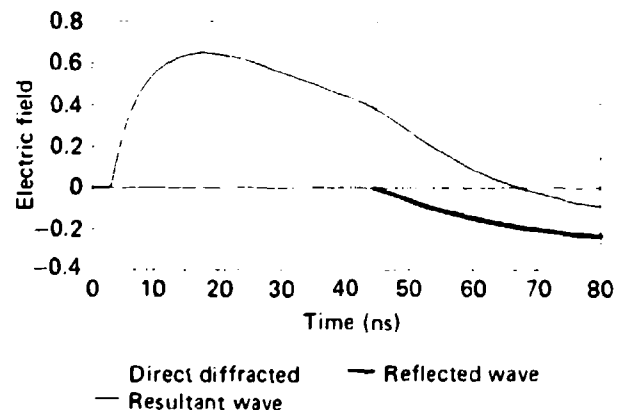


**Figure 28. Electric field with fence for observer height = 45.0 m.**

**Table 6. Theoretical peak field and ground delay as a function of observer height with fence**

Height (m)	$\bar{E}_f$	$T'_L$ (ns)
7.5	0.22	6.4
15.0	0.39	12.9
22.5	0.48	19.3
30.0	0.53	25.7
37.5	0.58	32.1
45.0	0.64	38.5

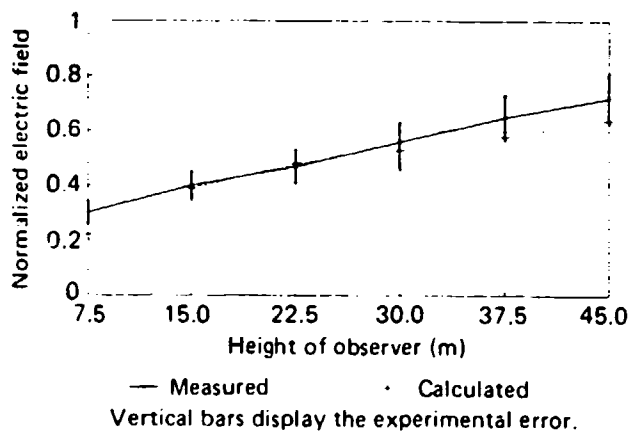


**Figure 29. Comparison between  $E_f$  and  $\bar{E}_f$  with fence.**

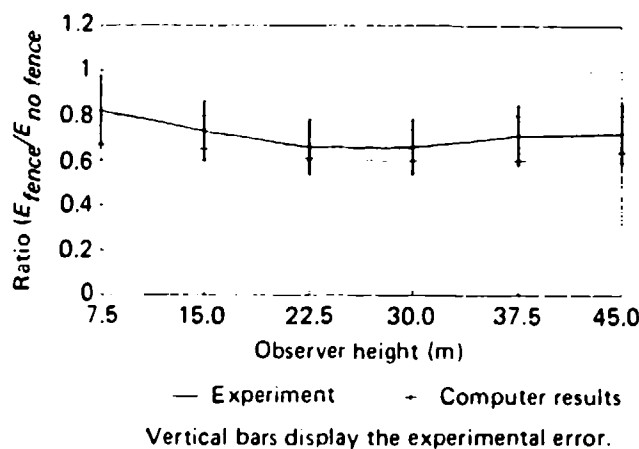


**Figure 30. Comparison between electric-field ratios.**

**Table 7. Comparison between experimental and theoretical electric-field ratios**

Height (m)	$E_f/E_N$	$\bar{E}_f/\bar{E}_N$	% difference*
7.5	0.82	0.67	18
15.0	0.73	0.65	11
22.5	0.66	0.61	8
30.0	0.66	0.60	9
37.5	0.71	0.60	15
45.0	0.72	0.64	11

$$*\% \text{ difference} = \frac{E_f/E_N - \bar{E}_f/\bar{E}_N}{E_f/E_N}$$

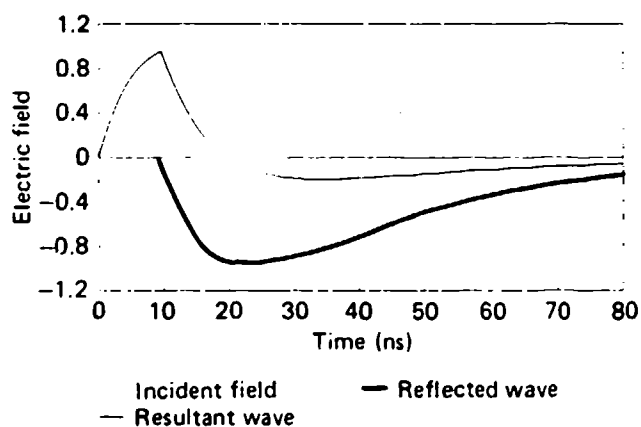


**Figure 31. Electric field in absence of fence, with 13.7-ns risetime and observer height = 22.5 m.**

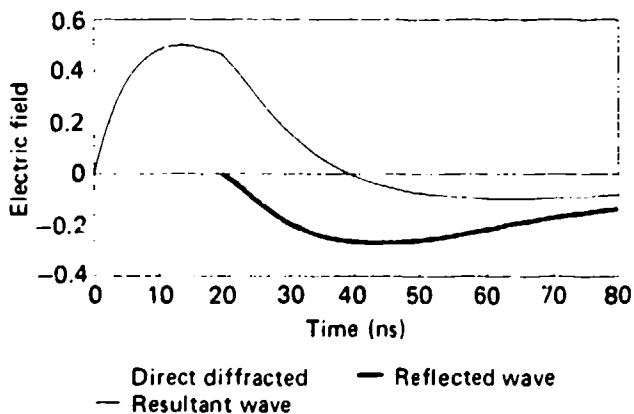


**Figure 32. Electric field with fence, with 13.7-ns risetime and observer height = 22.5 m.**

for waveforms of the AESOP regime. For shorter risetimes, with the same geometry, the improvement will reduce the ratio  $\bar{E}_F/\bar{E}_N$  to the 0.3 to 0.4 range.

In summary, the experimental results are in good agreement with Kohlberg's theoretical model [3].

## 5. Conclusions

The results of this scale model experiment allow us to assess the reduction of the fields of EMP simulators of the AESOP type that can be achieved with a totally reflecting fence placed around the perimeter of the test volume. The measured peak field, as a function of observer height, was found to be in good agreement with the theory. Typically, there was a 10-percent difference between the theoretical and experi-

mental results. The largest variation was 18 percent. We assume that closer agreement might have been achieved by more accurately matching the waveshapes and risetimes. This might be accomplished either in the scale-model pulse source, or by providing a variable waveshape input to the theoretical model.

It was shown that the fence did provide a reduction of the field in the region of interest, but the reduction was not especially large: around 50 percent.

The utility of using an EMP fence can be predicted by using the program FENCE. This program is executable on a PC in a few minutes. The waveshape, simulator-to-fence distance, fence-to-observer distance, and observer height are all used as variable inputs to the program. The effectiveness of a fence for many possible configurations can then be predicted.

## References

1. E. Patrick, *PREMPT Fort Huachuca Test Report*, Harry Diamond Laboratories, HDL-SR-76-2 (September 1976).
2. E. Patrick and S. Soo Hoo, *Transportable Electromagnetic (TEMPS) Preliminary Field Mapping Report*, Harry Diamond Laboratories, HDL-TM-74-15 (October 1974).
3. Ira Kohlberg, *Diffraction of Far Fields Produced by EMP Simulators due to a Wire Mesh Fence*, Kohlberg Associates, Inc., report KAITN003-88, contract DAAL02-87-C-0052 (July 1988).
4. I. Kohlberg and P. Elliot, *FENCE: A Computer Program for Determining the Diffracted Far Fields of EMP Simulators due to a Wire Mesh Fence*, Kohlberg Associates, Inc., report KAITN05-88, contract DAAL02-87-0052 (August 1988).
5. I. Kohlberg and P. Elliot, *REFLPROP: A Computer Program for Calculating the Time Behavior of an Electromagnetic Pulse Reflected from the Earth's Surface*, Kohlberg Associates, Inc., report KAITN004-88, contract DAAL02-87-0052 (July 1988).
6. G. Sinclair, *Theory of Models of Electromagnetic Systems*, Proc. IRE (November 1984), 1364-1370.
7. A. Cuneo and J. Loftus, *Scale Modeling for the Patriot Electromagnetic Pulse Test*, Harry Diamond Laboratories, HDL-TM-81-16 (May 1981).
8. A. Cuneo and J. Loftus, *Measurement of Scaled-Down High Altitude Electromagnetic Pulse (HEMP) Waveforms*, Harry Diamond Laboratories, HDL-TM-81-6 (March 1981).

## Appendix.—Experimental Error

The more simple the experiment, the lower the probability of error. The experiment described in the body of the report was simplified by using a substitution method for observing the effect of the fence on the horizontal electric field. The radiating dipole remained at a fixed position, while the recording field sensor was moved vertically at either of two fixed horizontal ranges. With the fields at each height recorded, the fence was immediately placed between the dipole and sensor and the measurements were repeated.

There is systematic error here, in that some changes will occur in the field strength and/or the measurement system between these two sets of measurements. We previously observed the measurement-system and/or field-strength variations by repeating the recording of the field at a given position several times. There was no more than a  $\pm 5$ -percent change in the peak of the recorded fields, with no significant change observed in the temporal distribution. This small deviation may be attributed to the measurement system's signal-averaging capability. Although it requires almost three minutes for the measurement system to average this signal 100 times, the number of pulsed fields which occurred during the acquisition is greater than 10,000. The averaging results in a signal-to-noise ratio increase of 10 and a significantly decreased importance in pulse-source shot-to-shot amplitude variation.

The computer-controlled aspect of the measurement system helps to minimize human errors, such as assigning a transfer function to a captured waveform. The data-collection program was

modified for this experiment so that the proper transfer function for the sensor was applied to the waveform by the computer each time data were collected. These data were observed for consistency of response on the CRT of the digital processing oscilloscope while the sampling and averaging was in process.

Other sources of error are the physical placement of the fence, elevation changes of the sensor, and the sensor alignment. The fence-placement error is considered to be  $\pm 3$  in., while the sensor-elevation error is placed at about  $\pm 0.5$  in. The effects of the fence-placement and elevation errors are quite small, in that they cause very little change to the slant range from the sensor to the dipole or from the sensor to the top of the fence (when the fence was present). The error introduced by sensor misalignment is also small, in that a  $10^\circ$  error would decrease the peak output by less than 3 percent. These physical placement (human) errors are assigned a value  $\pm 5$  percent.

We arbitrarily assign a random error of  $\pm 10$  percent because of undetected aspects such as measurement system gain fluctuation, variation in the electromagnetic environment, etc.

The experimental error for the data is approximated by the square root of the sum of the squares of the measurement-system/field-level estimation ( $\pm 5$  percent), the physical placement estimation ( $\pm 5$  percent), and the random error ( $\pm 10$  percent):

$$\begin{aligned} & (5^2 + 5^2 + 10^2)^{1/2} \\ & = \pm 13 \text{ percent.} \end{aligned}$$

# DISTRIBUTION

ADMINISTRATOR  
DEFENSE TECHNICAL INFORMATION CENTER  
CAMERON STATION, BUILDING 5  
ATTN DTIC-DDA (2 COPIES)  
ALEXANDRIA, VA 22304-6145

ASSISTANT TO THE SECRETARY OF DEFENSE  
ATOMIC ENERGY  
ATTN EXECUTIVE ASSISTANT  
WASHINGTON, DC 20301

DIRECTOR  
DEFENSE COMMUNICATIONS AGENCY  
ATTN CODE B410  
ATTN CODE B430  
WASHINGTON, DC 20305

DIRECTOR  
COMMAND, CONTROL, & ENGINEERING CENTER  
ATTN C-660  
ATTN G-630  
WASHINGTON, DC 20306

DIRECTOR  
DEFENSE COMMUNICATIONS ENGINEERING CENTER  
ATTN CODE R400  
ATTN CODE R123, TECH LIB  
ATTN CODE R111  
1860 WIEHLE AVENUE  
RESTON, VA 22090

ASSISTANT CHIEF OF STAFF FOR  
INFORMATION MANAGEMENT  
COMMAND SYSTEMS INTEGRATION  
OFFICE  
ATTN DAMO-C42  
THE PENTAGON  
WASHINGTON, DC 20301

DIRECTOR  
DEFENSE INTELLIGENCE AGENCY  
ATTN DB-4C2, D. SPOHN  
WASHINGTON, DC 20301

CHAIRMAN  
JOINT CHIEFS OF STAFF  
ATTN J-3  
ATTN C3S  
WASHINGTON, DC 20301

NATIONAL COMMUNICATIONS SYSTEM  
DEPARTMENT DEFENSE  
OFFICE OF THE MANAGER  
ATTN NCS-TS, D. BODSON  
WASHINGTON, DC 20305

DIRECTOR  
DEFENSE NUCLEAR AGENCY  
ATTN RAEV  
ATTN DDST

DIRECTOR  
DEFENSE NUCLEAR AGENCY (cont'd)  
ATTN RAEV  
ATTN TITL  
WASHINGTON, DC 20305

OFFICE OF UNDERSECRETARY OF  
DEFENSE RESEARCH & ENGINEERING  
DMSSO  
2 SKYLINE PLACE  
SUITE 1403  
5203 LEESBURG PIKE  
FALLS CHURCH, VA 22041

UNDER SECY OF DEF FOR RSCH & ENGG  
DEPARTMENT OF DEFENSE  
ATTN STRATEGIC & SPACE SYS  
9050 RM 3E129  
ATTN STRAT & THEATER NUC FORCES  
WASHINGTON, DC 20301

DEPUTY DIRECTOR FOR THEATRE/  
TACTICAL C3 SYSTEMS  
JOINT STAFF  
WASHINGTON, DC 20301

CAMMANDER-IN-CHIEF  
US FORCES, EUROPE  
ATTN ECC3S  
APO, NY 09128

ASSISTANT CHIEF OF STAFF FOR  
AUTOMATION & COMMUNICATIONS  
ATTN DAMO-C4T  
ATTN DAMO-C4S  
DEPARTMENT OF THE ARMY  
WASHINGTON, DC 20360

US ARMY BALLISTIC RESEARCH  
LABORATORY  
ATTN SLCBR-DD-T (STINFO)  
ABERDEEN PROVING GROUND, MD 21005

COMMANDER  
US ARMY INFORMATION SYSTEMS COMMAND  
ATTN CC-OPS-WR, O.P. CONNELL/ R. NELSON  
FT HUACHUCA, AZ 85613

US ARMY COMBAT SURVEILLANCE &  
TARGET ACQUISITION LABORATORY  
ATTN DELET-DD  
FT MONMOUTH, NJ 07703

COMMANDER  
US ARMY ELECTRONIC SYSTEMS ENGINEERING  
INSTALLATION AGENCY  
ATTN ASBH-SET-S  
FT HUACHUCA, AZ 85613

DISTRIBUTION (cont'd)

COMMAND  
US ARMY MATERIEL COMMAND  
ATTN DRCRE  
ATTN DRCDE  
5001 EISENHOWER AVE  
ALEXANDRIA, VA 22333-0001

DIRECTOR  
US ARMY MATERIEL SYSTEMS ANALYSIS  
ACTIVITY  
ATTN DRXSY-MP, LIBRARY  
ABERDEEN PROVING GROUND, MD 21005

DIRECTOR  
US ARMY MISSILE LABORATORY  
USAMICOM  
ATTN DRSMI-RPR, REDSTONE SCIENTIFIC  
INFO CENTER  
ATTN DRSMI-RPT, TECHNICAL  
INFORMATION DIV  
ATTN DRSMI-RN, CHIEF, TECHNOLOGY  
INTEGRATION OFFICE  
REDSTONE ARSENAL, AL 35809

COMMANDER  
US ARMY NUCLEAR & CHEMICAL AGENCY  
ATTN MONA-WE  
7500 BACKLICK ROAD  
SPRINGFIELD, VA 22150

DEPT CH OF STAFF FOR RSCH, DEV, & ACQ  
DEPARTMENT OF THE ARMY  
ATTN DAMA-CSS-N  
WASHINGTON, DC 20310

CHIEF  
US ARMY SATELLITE COMMUNICATIONS  
AGENCY  
ATTN DRCPM-SC  
FT MONMOUTH, NJ 07703

COMMANDANT  
US ARMY WAR COLLAGE  
ATTN LIBRARY  
CARLISLE BARRACKS, PA 17013

COMMANDER-IN-CHIEF  
ATLANTIC  
ATTN J6  
NORFOLK, VA 23511

COMMANDER  
NAVAL ELECTRONIC SYSTEMS COMMAND  
ATTN PME 110-241D  
WASHINGTON, DC 20360

CHIEF OF NAVAL MATERIEL  
THEATER NUCLEAR WARFARE  
PROJECT OFFICE  
ATTN PM-23  
WASHINGTON, DC 20360

COMMANDING OFFICER  
NAVAL RESEARCH  
LABORATORY  
ATTN CCDE 4720, J. DAVIS  
WASHINGTON, DC 20375

COMMANDER  
NAVAL SURFACE WEAPONS CENTER  
ATTN TECH LIBRARY  
DAHLGREN, VA 22448

COMMANDER  
NAVAL SURFACE WEAPONS CENTER  
ATTN TECHNICAL LIBRARY  
WHITE OAK LABORATORY  
SILVER SPRING MD 20910

AIR FORCE COMMUNICATIONS COMMAND  
ATTN EPPD  
SCOTT AFB, IL 62225

AIR FORCE WEAPONS LABORATORY/DYC  
ATTN TECH. LIBRARY  
KIRTLAND AFB, NM 87117

LAWRENCE LIVERMORE NATIONAL LIB  
ATTN TECHNICAL INFO DEPT LIBRARY  
PO BOX 808  
LIVERMORE, CA 94550

DIRECTOR  
NATIONAL SECURITY AGENCY  
ATTN R15  
9800 SAVAGE ROAD  
FT MEADE, MD 20755

BDM CORP  
ATTN CORPORATE LIBRARY  
7915 JONES BRANCH DRIVE  
MCLEAN, VA 22102

BOEING CO  
ATTN TECH. LIBRARY  
PO BOX 3707  
SEATTLE, WA 98124

ENGINEERING SOCIETIES LIBRARY  
ATTN ACQUISITIONS DEPT  
345 E. 47TH ST  
NEW YORK, NY 10017

ENSCO, INC  
ATTN R. GRAY  
540 PORT ROYAL RD  
SPRINGFIELD, VA 22151

IIT RESEARCH INSTITUTE  
ATTN TECH. LIBRARY  
10 W 35TH STREET  
CHICAGO, IL 60616

DISTRIBUTION (cont'd)

INTERNATIONAL TEL & TELEGRAPH CORP  
ATTN TECHNICAL LIBRARY  
500 WASHINGTON AVENUE  
NUTLEY, NJ 07110

MARTIN MARIETTA CORPORATION  
ATTN DR. C. WHITESCARVER  
PO BOX 5837  
ORLANDO, FL 32805

MISSION RESEARCH CORP  
ATTN DR. W. STARK  
4935 N 30TH STREET  
COLORADO SPRINGS, CO80933

MISSION RESEARCH CORP  
ATTN J. DANDO  
ATTN DR. H. ROBERTS  
3103 FOX DEN LANE  
OAKTON, VA 22124

MISSION RESEARCH CORP  
EM SYSTEM APPLICATIONS DIVISION  
ATTN TECHNICAL LIBRARY  
1720 RANDOLF ROAD, SE  
ALBUQUERQUE, NM 87106

ROCKWELL INTERNATIONAL CORP  
ATTN D/24-068, 031-CA31  
PO BOX 3105  
ANAHEIM, CA 92803

SRI INTERNATIONAL  
ATTN TECH. LIBRARY  
333 RAVENSWOOD AVENUE  
MENLO PARK, CA 94025

TRW DEFENSE & SPACE SYSTEMS GROUP  
ATTN J. PENAR  
ONE SPACE PARK  
REDONDO BEACH, CA 92078

TRW, INC  
COMMAND & CONTROL & COMMUNICATIONS  
SYSTEM DIV  
ATTN N. STAMMER  
5203 LEESBURG PIKE  
SUITE 310  
FALLS CHURCH, VA 22041

US ARMY LABORATORY COMMAND  
ATTN TECHNICAL DIRECTOR, AMSLC-TD

INSTALLATION SUPPORT ACTIVITY  
ATTN LEGAL OFFICE, SLCIS-CC

USAISC  
ATTN RECORD COPY, AMSLC-IM-TS  
ATTN TECHNICAL REPORTS BRANCH,  
AMSLC-IM-TR (3 COPIES)

HARRY DIAMOND LABORATORIES  
ATTN D/DIVISION DIRECTORS  
ATTN LIBRARY, SLCHD-TL (3 COPIES)  
ATTN LIBRARY, SLCHD-TL (WOODBIDGE)  
ATTN CHIEF SCIENTIST, SLCHD-CS  
ATTN DEPUTY DIRECTOR, SLCHD-NW-E  
ATTN SPECIAL PROJECTS OFFICER, SLCHD-NW-E  
ATTN CHIEF, SLCHD-NW-EP  
ATTN CHIEF, SLCHD-NW-EP (15 COPIES)  
ATTN CHIEF, SLCHD-NW-ES  
ATTN CHIEF, SLCHD-NW-TN  
ATTN CHIEF, SLCHD-NW-CS  
ATTN CHIEF, SLCHD-NW-RP  
ATTN CHIEF, SLCHD-NW-TL  
ATTN CHIEF, SLCHD-NW-RS  
ATTN CHIEF, SLCHD-NW-P  
ATTN CHIEF, SLCHD-TT  
ATTN CHIEF, SLCHD-TA  
ATTN CHIEF, SLCHD-TL  
ATTN W. L. VAULT, SLCHD-NW  
ATTN M. BUMBAUGH, SLCHD-NW-RS  
ATTN Z. G. SZTANKAY, SLCHD-ST-SP  
ATTN J. LOFTUS, SLCHD-NW-EH (30 COPIES)